Theor Appl Climatol
DOI 10.1007/s00704-008-0074-9

ORIGINAL PAPER

# MODIS/Terra observed snow cover over the Tibet Plateau: distribution, variation and possible connection with the East Asian Summer Monsoon (EASM)

**Zhaoxia Pu · Li Xu**

Received: 7 July 2008 / Accepted: 13 October 2008


**Abstract** Based on the snow cover fraction (SCF) data acquired from the Moderate Resolution Imaging Spectroradiometer (MODIS) on the NASA Terra spacecraft from 2000–2006, statistical analyses are performed to explore the spatial and temporal distribution and variation of the snow cover over the Tibetan Plateau (TP). It is found that the snow persistence over the TP varies in different elevation ranges generally becomes longer with increases in the terrain elevation. In addition, the spatial distribution of the snow cover not only depends on the elevation but also varies with terrain features, such as aspect, slope, and curvature in the local areas. With 7-year observational data, seasonal and interannual variability of snow cover has been detected. There are slight decreasing trends in SFCs from 2000–2006. With MODIS satellite snow-cover fraction data and the National Centers for Environmental Predictions and U.S. Department of Energy NCEP/DOE reanalysis II dataset, the relationship between snow cover anomalies over the TP and the East Asian Summer Monsoon (EASM) is examined. Results indicate that the onset of the EASM is closely associated with snow cover anomalies in the spring. Specifically, a positive (negative) snow cover anomaly is followed by a later (earlier) onset of the EASM.

## 1 Introduction

The Tibetan Plateau (TP), or Qinghai-Xizang (Qingzang) Plateau is the highest and largest plateau in the world. It covers an area of 3.6 million km$^2$ 2,000 m above the mean sea level (MSL), of which 59% are 4,000 m above MSL. Thus, it is commonly called “the roof of the world”. It has been recognized that uplifted plateau exerts a profound dynamic and thermal forcing on the regional atmospheric circulation (Yeh et al. 1979; Yanai et al. 1992).

Compared with other regions in the same latitudes (25–40°N), seasonal snow cover over the TP is a notable characteristic in global snow maps. Snow cover can persist at higher altitude regions during all seasons. Thus, it exerts a significant thermal forcing on the local atmosphere general circulation (Li 1993). Previous studies have indicated that seasonal snow cover over the TP is a comprehensive indicator of the mean conditions of temperature and precipitation in the area and its surroundings (Hahn and Shukla 1976; Dickson 1984; Yang 1996). Snow cover and glacier over the TP also respond to global warming, thus it is an important issue in climate change studies (Qin et al. 2006). Moreover, the seasonal snow cover is speculated as being an important factor in regulating the Asian monsoon. The anomalous snow cover will influence the energy and water exchange between the land surfaces and the lower troposphere by modulating radiation, water and heat flux (Cohen and Rind 1991). Therefore, snow cover anomalies have been suggested as a potential predictor of the Asian monsoon in some previous studies (Hahn and Shukla 1976; Dey et al. 1985; Dickson 1984; Parthasarathy and Yang 1995; Yang 1996; Sankar-Rao et al. 1996), in addition, it is believed that the snow cover over the TP exerts an influence on the summer rainfall over East Asia (EA). Moreover, snow cover over the TP is a vital water source for the western and northern parts of China. The largest rivers in China, such as the Yangtze River, Yellow River, etc., have their headwaters there. Therefore, study of the snow cover over the TP and its seasonal variations become a very important scientific problem.

Z. Pu (✉) · L. Xu
Department of Meteorology, University of Utah,
135 S 1460 E, Room 819,
Salt Lake City, UT 84112, USA
e-mail: Zhaoxia.Pu@utah.edu

However, before the era of "satellite meteorology", traditional sources of snow observations were usually obtained from ground-based meteorological networks, in which only the presence or absence of snow along with snow depth is measured on a daily basis. At present, there are only 115 conventional ground-based stations managed by the Chinese government over the TP (Fig. 1). Most of these stations are located in the inhabited lower-altitude river valleys, where elevations are usually below 4,500 m. Given the scarcity of ground-based, in-situ stations, it is difficult to adequately capture the spatial variability in snow cover. Therefore, complete and accurate snow cover information over the TP is difficult to obtain. Due to this difficulty, the detailed distribution and variability of snow cover in the TP has not yet been fully explored. Most of the previous studies were based on limited amount of in-situ snow depth observations (e.g., Wu and Qian 2003; Qin et al. 2006).

With advances in remote-sensing technology, satellite-derived snow cover information has become an alternative data source. For instance, weekly snow mapping of the northern hemisphere using National Oceanographic and Atmospheric Administration (NOAA) National Environmental Satellite, Data and Information Service (NESDIS) data began in 1966. This snow cover data is one of the longest, if not the longest satellite record of an important climatological variable, and it has been studied intensively by Frei and Robinson (1999). Guo et al. (2004) compared the NESDIS weekly snow product with ground snow depth observations over China in past 30 years. They found significant differences between the NESDIS snow mapping and in-situ Chinese ground-based observations and concluded that the NESDIS snow-cover products tend to overestimate snow cover over the TP. They attribute the cause of the overestimation to the coarse spatial resolution (total of 89×89 grids over the northern hemisphere) of the NESDIS data, wherein the data do not represent well the detailed information of patchy and shallow snow cover over the TP and, instead, just call such areas completely snow covered.

Another important source of snow water equivalent (SWE) information is passive microwave remote sensing (Chang et al. 1987, 1990). With a single global algorithm to extract snow depth from the SMM/I and SMMR, microwave-derived estimations seriously overestimate the snow depth over the TP (Che et al. 2004). Specifically, the microwave retrievals show large errors in shallow and wet snow. Other merged snow cover datasets, such as the National Snow and Ice Data Center's (NSIDC) Northern Hemisphere Snow Extent dataset (Armstrong and Brodzik 2001), are largely based on the NOAA/NESDIS mappings and the SWE derived from passive microwave remote sensing, showing the same problems over the TP.

On December 18, 1999, the National Aeronautics and Space Administration (NASA) Earth Observing System (EOS) Terra satellite was launched with a complement of five instruments, one of which is the Moderate Resolution Imaging Spectroradiometer (MODIS). Among all the comprehensive observations on cloud, ocean, and earth surface characteristics available from the Terra MODIS (Hall et al. 2002a; Jin 2006; Qu et al. 2006), the snow cover product is available since February of 2000. With improved spatial resolution (500 m globally), high temporal frequency (daily), enhanced capability to separate snow and clouds (Hall et al. 2002b) due to more spectral bands (particularly in the short-wave infrared), as well as a consistently applied, automated snow-mapping algorithm (Riggs et al. 2003), MODIS provides an excellent opportunity to study the snow cover over large, relatively inaccessible regions such as the TP.

Pu et al. (2007) evaluated the accuracy of the MODIS/Terra snow cover data products over the TP by comparing the MODIS 8-day composite snow data product (i.e., Level 3 data at 500-m resolution, Riggs et al. 2003) with in-situ

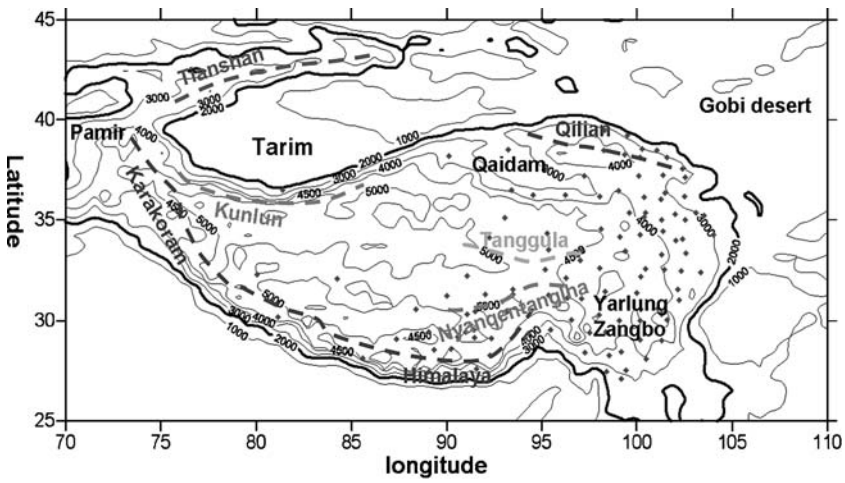


**Fig. 1** Map of the Tibetan Plateau area. The contour lines (interval: 1,000 meters) show the elevation of topography in the area. Available in situ ground-based stations are shown as *dots*. The thicken contour line represents the elevation at 2,000 m

Chinese ground-based station snow observations from 115 ground-based stations over the TP from 2001–2003. Results show that the overall accuracy of MODIS snow data is about 90% over the TP area. Total error in these observations over the TP is about 10% and this compares favorably with previous studies showing global average errors of 8% (Hall et al. 2002b). The major omission errors are likely caused by occasions when the snow was quite shallow or snow cover events that were short in duration. Since 8-day composite snow cover fraction (SCF) data products at climate model grids (0.05×0.05 -resolution, about 5 km) are directly derived from the snow data at 500-m resolution, statistical analysis is then performed over the MODIS snow data from 2000–2006 to examine the seasonal variation of the SCF over the TP. They found that the most persistent snow cover is located in the southern and western edges of the TP within large mountain ridges and western part of Yarlung Zangbo valley. The duration for snow persistence varies in different elevation ranges and generally becomes longer with increases in the terrain elevation.

As an extended study of Pu et al. (2007), in this study we further examine the temporal and spatial distribution and variation of the snow cover over the TP based on the MODIS/Terra satellite data from 2000–2006. In addition, since previous studies suggested that there might be a connection between winter snow cover over the TP and summer rainfall over East Asia during the monsoon season (e.g., Zhang and Tao 2001; Wu and Qian 2003), the possible connection between snow cover over the TP and the East Asian Summer Monsoon (EASM) will also be examined.

The paper is organized as follows. Section 2 briefly describes the MODIS snow mapping and terrain data used in this study; Sections 3 and 4 present the seasonal variation of the snow cover over the TP and snow cover distribution with various terrain features. Section 5 shows the interannual variations and anomalies of the snow cover. Section 6 examines the connection between the snow cover anomalies over the TP and the EASM onsets. Summary and discussion are drawn in Section 7.

## 2 Data

### 2.1 MODIS snow mapping

MODIS is a 36-channel visible-to-thermal-infrared sensor that was launched as part of the EOS Terra payload on December 18, 1999. Various snow and ice products are produced with MODIS imagery and the data are available at a variety of spatial and temporal resolutions (Hall et al. 2001). Considering the fact that the snow cover over a certain area is frequently, if not always, referred to the fraction of snow covered land, in this study, the 8-day composite of SCF data in 0.05° x 0.05° climate modeling grid (MOD10C2) datasets are used. Compared with the daily snow-cover products, the eight-day composite of snow cover maps greatly reduce the percent of cloud obscured or masked pixels from near half to less than 7% over TP (Hall et al. 2001; Riggs et al. 2003). Furthermore, the 8-day composite of data products cover the whole TP area without any missing data due to orbit swaths. The snow-cover fraction (SCF) provided by MOD10C2 in each CMG grid is defined as:

$$f_{snow} = \frac{n_{snow}}{n} \times 100 \quad (1)$$

where $n$ is the total number of pixels (at 500-m resolution) in a CMG grid mesh:

$$n = n_{snow} + n_{clear\_land} + n_{cloud\_obscured} + n_{unknown} \quad (2)$$

$n_{\text{snow}}$ is the total pixels identified as snow in this grid, $n_{\text{clear\_land}}$ for snow-free land, $n_{\text{cloud\_obscured}}$ for cloud and $n_{\text{unknown}}$ for other types of land.

As shown in the previous evaluation (Pu et al. 2007), the commission error (false alarm) of MODIS snow mappings is larger than the omission error over the TP. As a result, the snow algorithm would overestimate the snow cover in 500-m pixels. However, the magnitude of underestimation due to cloud obscuration roughly compensates overestimation due to commission error (Riggs et al. 2003). Thus, the SCFs at CMG derived from the high-resolution 500-m observations provide an excellent opportunity to quantitatively analyze the snow cover over the TP.

### 2.2 Digital elevation model data

The elevation data used in this study were obtained from the USGS GTOPO30 Digital Elevation Model (DEM) dataset (http://edc.usgs.gov/products/elevation/gtopo30/gtopo30.html). The resolution of elevation data in GTOPO30 is 30-arc seconds (approximately 1 km at the equator). We re-sampled the 30-arc seconds GTOPO30 data to 0.05° CMG grid by area average in accordance with the resolution of MODIS SCFs at CMG.

We specifically define the area of the TP as the region covering about 3.6 million km$^2$ with an elevation *higher* than 2,000 m (Pu et al. 2007). This overall area occurs in a domain between 70 and 110°E longitude and 25–45°N latitude. Major mountain ridges in the region include the Himalaya Mountains in the southern edge of the TP, and the Caracara and Kunlun mountains in the western and northern edges. The Pamir, Karakoram, Kunlun and Tianshan ridges are adjacent in the west part. The Qilian Mountain separates the Gobi desert from the TP in the

northeastern edge. Two large sub-regions, the Qaidam basin and Yarlung Zangbo valley, are located in the east-northern and east-southern part of the TP, respectively (Fig. 1).

## 3 Seasonal variations and distributions

### 3.1 Seasonal snow cover distributions

Seasonal mean SCF was obtained by the weight averaging of eight-day MOD10C2 data for each season from 2000–2006. Figure 2 shows the seasonal mean of SCF over the TP in four seasons. Extreme inhomogeneous spatial distribution and variability are exhibited due to the complex terrains over the TP. Specifically, higher SCFs correspond well with the huge mountains, including Himalayas, Karakoram, Pamirs, Kunlun and Nyainqentanglha Mountains. The most persistently snow covered areas (SCF larger 50%) are concentrated in the Himalayas, Kunlun, Karakoram ranges and the western part of the Yarlung Zangbo Valley, especially in the combined areas of Karakoram and Kunlun Mountains where the most heavily glaciated regions in the world are located, outside of the Polar region. In the southeast of the TP, SCF is also relatively higher because moist air rises along the Yarlung Zangbo Valley from the southern region. In contrast, due to large-scale shielding from the Himalaya and Karakoram mountains, most of the interior of the TP has relatively less snow cover persistence, although the averaged elevation is beyond 4,000 m. In the summer, there is scattered patchy snow cover in the high elevated regions along the Himalayas, Karakoram, and Kunlun ranges.

Figure 3 shows the annual percentage of large SCF over the TP, defined as the percent of days annually in which SCF is larger than 50% over five complete snow years. The highest percentages are concentrated in the Himalayas, Kunlun, Karakoram and the western part of Yarlung Zangbo valley, which is consistent with the larger SCF regions in the winter and spring. Especially in the coalesced region of the Karakoram and the Kunlun Mountain the frequency is larger than 70%. In the southeastern part of TP, the frequency is also relatively high due to the moist airflow that goes up along the Yarlung Zangbo valley from the Indochina Peninsula. Most of the interior TP has a lower frequency of the large SCF. Only in very high mountains, such as the Nyainqentanglha Mountain, is the frequency relatively higher than in the nearby region. In the Qaidam basin, the frequency of heavy snow cover is lowest. In the area of elevation within 2,000–4,000 m, the median duration of more than 50% in SCF is about 22 days, compared to 56 days in region of 4,000–6,000 m and 195 days in the region of above 6,000 m.

The distribution of snow cover is strongly linked to the available moisture over the Tibetan plateau. Based on the National Centers for Environmental Predictions and U.S. Department of Energy (NCEP/DOE) reanalysis data II (Kanamitsu et al. 2002) from 1979 to 2002, the available precipitable water in the southern flank of TP comes from

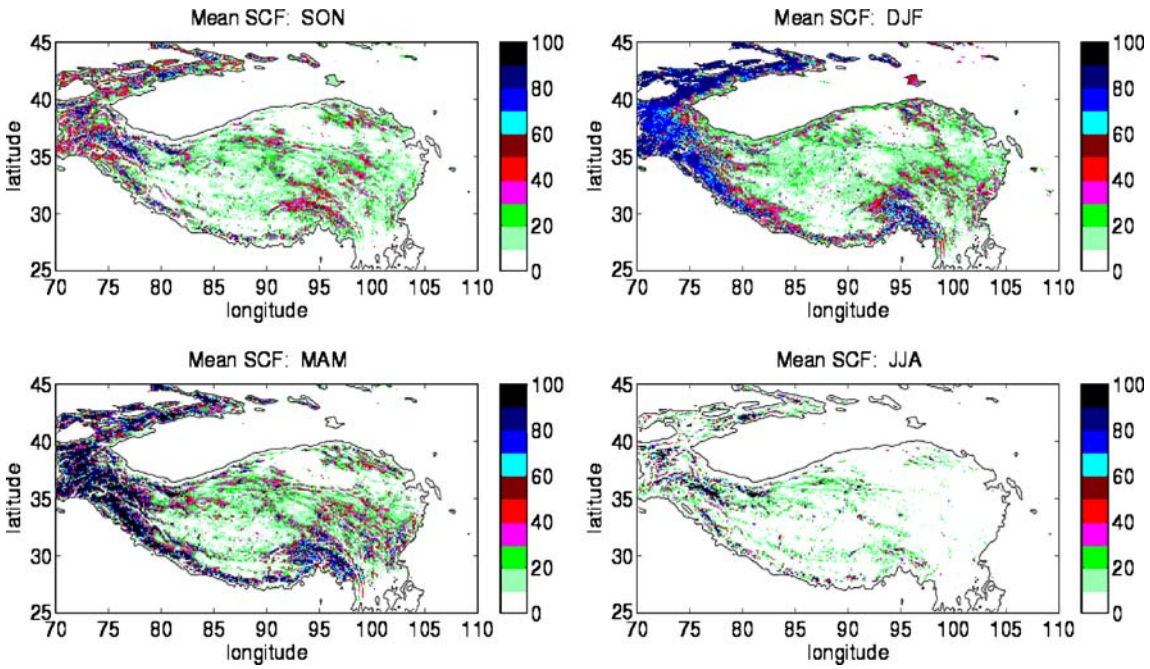


**Fig. 2** Seasonal mean of snow cover fraction (SCF) over the TP in the fall (September to November, SON), winter (December to February, DJF), spring (March to May, MAM) and summer (June to August, JJA) from 2000–2006

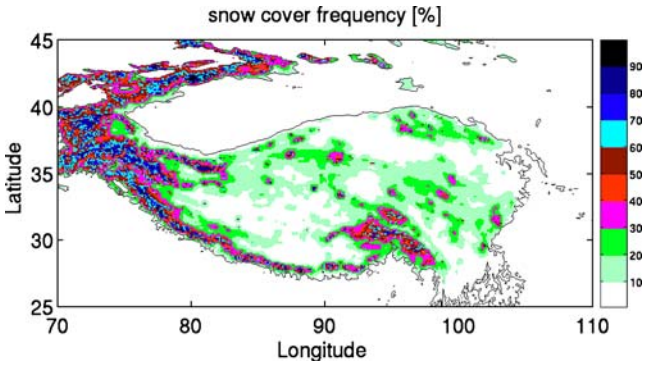


**Fig. 3** The annual percentile frequency of large snow cover fraction (SCF>50%). The statistics are based on five complete snow years from 2001 to 2005

the tropical ocean in the south, including the Indian Ocean and the Arabian Sea. The total column precipitable water content is relatively large in the winter along the west-southern flank of TP, decreasing dramatically from above 10 kg/m$^2$ to near zero along the Himalayas and Karakoram (figure not shown). Specifically, the Pamirs and Tibetan Plateau form a horn-shape village in the western part of Himalaya, which further enhances the convergence of moisture and terrain precipitation in the western edge of TP. Due to the huge shielding effect by the Himalayas and the Karakoram, there is little moisture in the vast interior of TP. In particular, the precipitable water is near to zero in the center of TP, corresponding to the area with less of a SCF in the winter. On the other hand, the available moisture in the northern flank of TP is mainly conveyed from remote Atlantic and Arctic oceans by westerly flow, contributing to most of the snowfall in Tianshan region. In the winter, large-scale vertical motion over the TP descends, which also greatly contributes to the sublimation of the snow in the interior of the TP.

### 3.2 Monthly mean and annual cycle

The 8-day composite snow cover data are aggregated to obtain monthly mean SCF using a weighted average from available data during period from 2000 to 2006. Figure 4 shows the annual cycle of monthly SCF mean in the different elevation ranges. Strong seasonal variations in SCF are found over the whole area of the TP. The maximum monthly mean SCF over the entire TP is roughly 33% in February. During snow season (early October to late April), the mean SCF over the TP is greater than 23%. After May, the mean SCF decreases rapidly and reduces to 5.3%. From September, the mean SCF increases rapidly and reaches a relative stable level in the early November.

The annual cycle of snow cover also depends on elevation heights. Specifically, the patterns of the annual cycle are pretty similar for elevations below 5000 m. Above 5000 m, the snow season and snow cover duration is relatively longer. Specifically, at the elevations above 6,000 m (Fig. 4), averaged SCFs are greater than 50% in all seasons, with two peaks of maximum SCF in late October and early May and a relative minimum during early of December to later of January along with the typical minimum in the summer.

The two SCF peaks above 6,000 m of elevation height may reflect the snow frequencies at high altitudes and also a possible negative (self-regulating) snow-cover feedback as suggested by Walland and Simmonds (1997): with sudden SCF increases after a snow storm in November, the air temperature in the lower troposphere decreases and

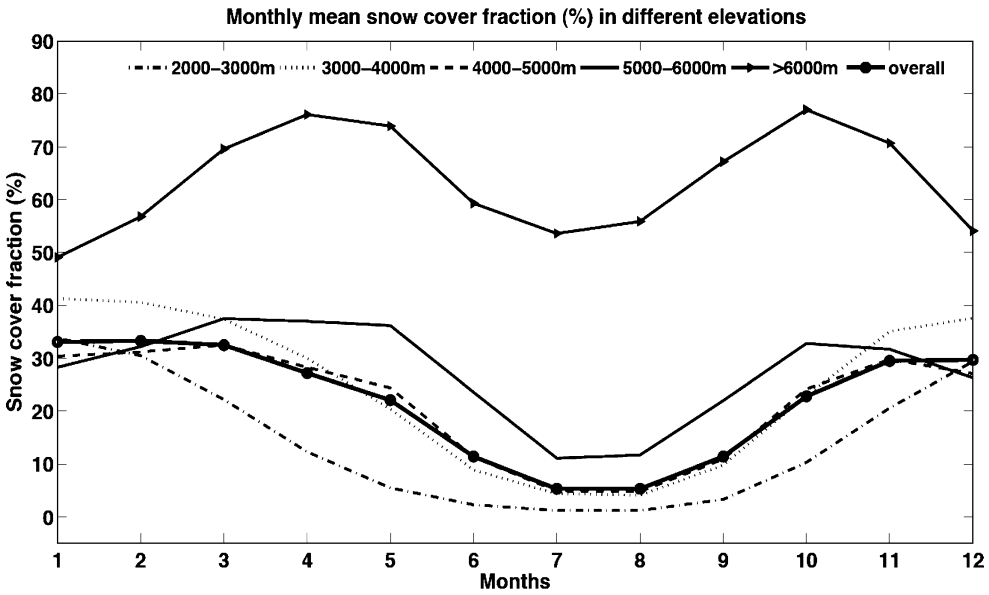


**Fig. 4** Monthly mean snow cover fraction (%) averaged over a 7-year period (2000–2006) at different elevation ranges

static stability of atmosphere increases. This leads to a reduction in the probability of later snowfall. The reduction of snowfall further results in decreasing SCF by snow blowing event and sublimation in the winter. The decreased SCF in land surface corresponds to increases of the sensible heating to the atmosphere and decreases the static stability thus the probability of snowstorms would increase in March. This negative feedback keeps the snow cover relatively stable over the TP in the winter.

Furthermore, blowing snow events caused by strong westerly winds at upper levels (i.e., East Asia Jet Stream, Moore 2004) in the winter cause the reduction of SCF in the high elevation regions. Sublimation also contributes significantly to decreases in SCF during the winter, especially in the areas with thin snow cover (Qin et al. 2006).

## 4 Spatial distribution and seasonal variations based on the terrain features

The annual cycle and monthly mean mentioned above indicate that the snow cover distribution depends on the terrain height over the TP. Distribution of the SCF over the mountainous areas also typically varies with the terrain features, such as slope, aspect and curvature in the local areas. In a geographic context, slope is defined as the angle of topographic surface to the horizontal plane, and aspect refers to the direction of the incline. The slope indicates the steepness of terrain, usually shown in the upward angles from the horizon. The curvature measures the second derivative of elevation at each cell, akin to the slope of the slope, which is used to describe the convex/concave characteristics of the terrain. A positive curvature indicates that the surface is upwardly convex in the cell and a negative curvature indicates that the surface is upwardly concave. A value of zero indicates that the surface is flat.

Figure 5 shows a histogram of the elevation, slope, aspect, and curvature distribution over the TP. The distribution of elevation is not uniform over the TP with a larger fraction of the area between 4,000 and 5,000 m MSL, roughly 40%. The area between 2,000 and 3,000 m occupies 20.2% of the total area of TP, and the area between 3,000 and 4,000 m for 21.2%, 5,000 and 6,000 m for 18.5% and above 6,000 m for 0.3%, respectively.

Meanwhile, the steeper mountains (higher slopes) are concentrated along the southern and western edge of the TP, especially in the Himalayan and Karakoram ranges (figure not shown). These two huge mountain ranges act as a large shield that separates the tropical monsoon climate in the Indian Peninsula and continental/micro-thermal climate in northwestern China. In the interior of the TP, the slope is small, although the average altitude is 4,000 m above the MSL.

To study the snow-cover distribution from different perspectives, the slopes are classified into four categories: northward slopes (315< aspect <45), eastward slopes (45< aspect <135), southward slopes (135< aspect <225) and westward slopes (225< aspect <315). Over the TP, the slopes are commonly southward in the southern edge of the plateau, while the slopes are commonly northward in the northern edge. In the interior of the plateau, the aspects are extremely inhomogeneous. In the whole TP, the northward slope occupies roughly 30%, eastward slope 23%, southward slope 26%, and westward slope 21%, respectively. In addition, the concave and convex terrains are located coherently with huge mountains and valleys near the outline of TP. In the interior of the TP, the curvatures are predominantly near zero (figure not shown).

In the following sections, we examine the dependence of the SCF distribution and variation with the terrain features.

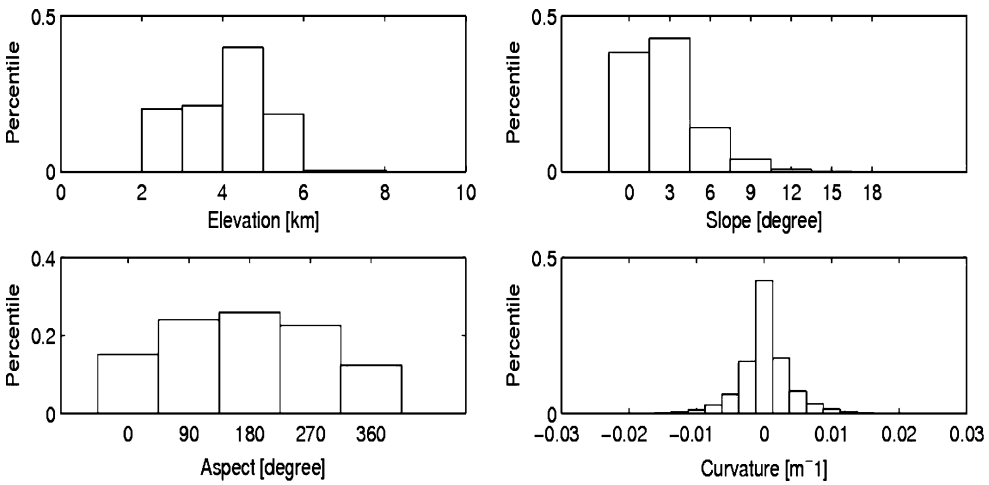


**Fig. 5** Histogram of elevation (units: m), slope (units: degree), aspect (units: degree) and curvature (units: $m^{-1}$) over TP. The number in the *x*-axis is the center value in each bin for the variable. The *y*-axis is the ratio in each bin

### 4.1 Aspect

Figure 6 displays the mean SCF associated with the different aspects over the TP during four typical months of the snow maximum (February), ablation (May), minimum (August), accumulation (November) seasons. The radius in the polar coordinate indicates the value of SCF (units: %), and angle indicates the aspect (units: degree). Three curves in each panel are the mean SCF in the area of 2,000–4,000 m, 4,000–6,000 m and above 6,000 m, respectively.

As seen from the figures, the snow-cover fraction in the southward and eastward slope is relatively larger than that in the northward and westward slope at the same elevation. This feature contradicts common sense: the southward slopes receive more solar radiation, which would cause a significant reduction in the snow cover of the southward slope. The difference in the SCF between the southward and northward slope is perhaps a result of the configuration of air moisture and huge terrain. Most of the air moisture is conveyed from the tropical region in the south of the TP, which leads to intensive snowfall caused by terrain/orographic lifting in the southward slope along the southern edge of the TP. The northward slope receives less snowfall during autumn and winter. Although it receives more solar radiation in the southward slope, the snow-albedo effect could maintain a relatively large SCF in that aspect. In addition, the westerly jet stream over the TP will seriously reduce the SCF in the upwind (westward) slope by blowing snow. These factors may contribute to the difference between the westward and eastward slopes.

The difference in snow cover within the areas of elevation range of 2,000–4,000 m and 4,000–6,000 m is evident in Fig. 6. In the snow accumulation season (November) and maximum season (February), the SCF in the area of 2,000–4,000 m (line) is bigger than SCF in the elevation 4,000 m–6,000 m (dash). But in the snow ablation season (May) and the minimum season (August), the SCF in the area of 2,000–4,000 m is smaller. This inversion in SCF is the result of the distribution of elevation. The majority of area below 4,000 m is located on the border (edge) of the TP where the SCF in autumn and winter is larger than that in the interior of the TP due to the orographic lifting; whereas most of the area between 4,000 and 6,000 m is located in the interior of the TP, where the snow cover fraction is small but could persist for a longer period.

### 4.2 Slope

Figure 7 shows the mean SCF variation as a function of slope within the different aspects during the similar four stages (i.e., maximum, ablation, minimum and accumulation in February, May, August, and November). Regardless of the steepness of the slopes, the snow-cover fraction is relatively larger in the southward and eastward slopes. With

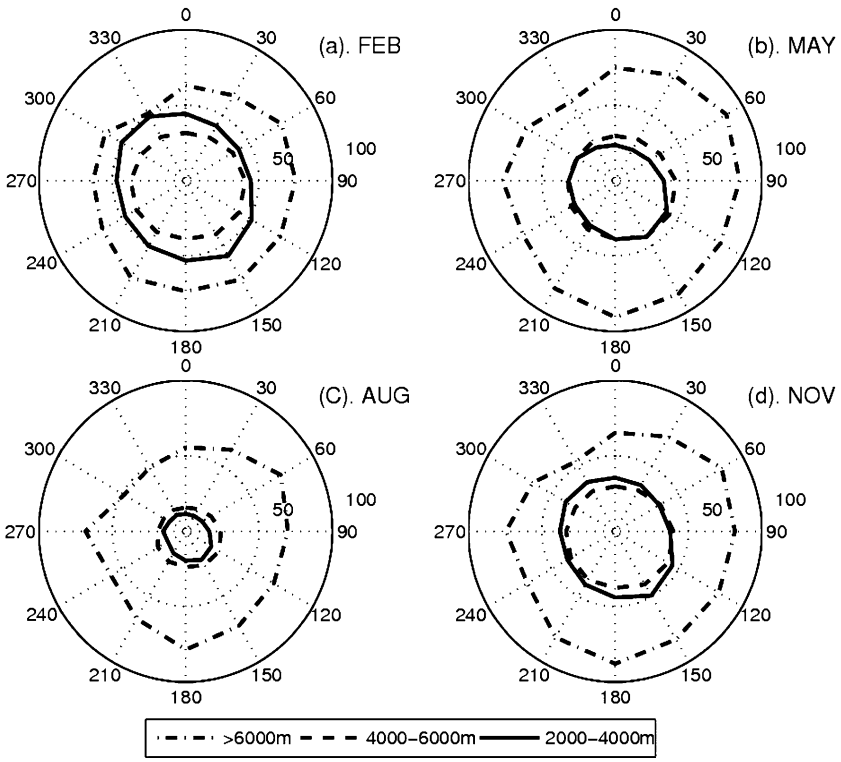


**Fig. 6** Mean SCF in the different aspects over TP during the snow maximum season (February), the ablation season (May), the minimum season (August), and the accumulation season (November). The radius in the polar coordinate demonstrates the SCF (units: %), and the angle indicates the aspect (units: degree). The three curves are the mean SCF in the area of 2,000–4,000 m, 4,000–6,000 m and above 6,000 m, respectively

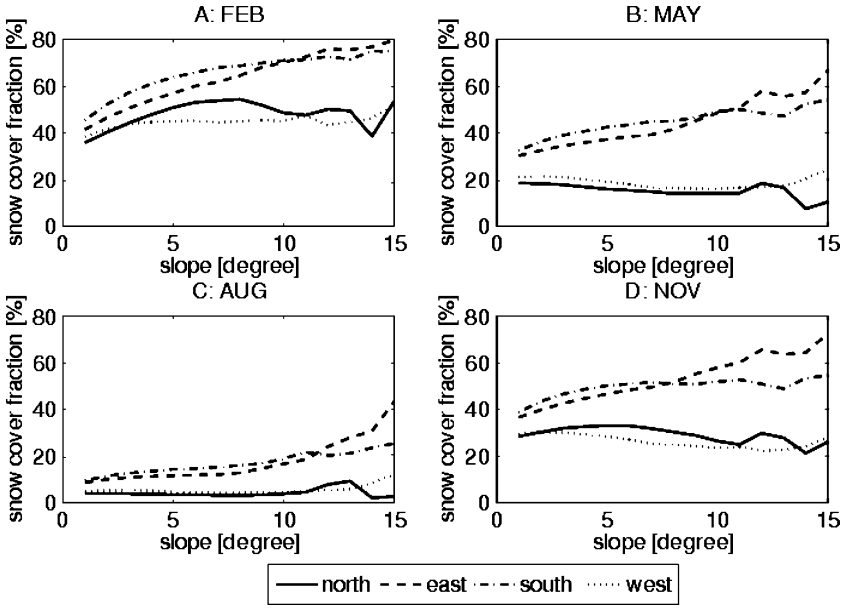


**Fig. 7** Mean SCF as a function of slope in the different aspects during the snow maximum season (February), the ablation season (May), the minimum season (August), and the accumulation season (November). The *x*-axis is the slope in degree and the *y*-axis is the snow cover fraction in percent

increasing slope, the average SCF increases on the southward and eastward slopes. In contrast, the SCF keeps a relatively constant value or even a slight decrease in the northward and westward slope. This feature is also a possible result of the uplifting of air moisture along the southern and western edge of the TP. In the snow maximum season (February), the SCF does not show much difference in the flat slopes (slope <5°). With increasing slope, the SCF in southward and eastward grows rapidly.

The average SCF in the eastward slope is larger than the southward slope when the slope is larger than 10° but there is a systematic inversion of this trend when the slope is lower than 10°. This feature is more evident in the snow minimum season (Fig. 7c). A possible reason is that the southward slope receives more solar radiation than the eastward slope, leading to the largest SCF in the summer to be located on the steep east-facing mountain. Snow cover in the northward and westward slopes is not sensitive to the slope. In the ablation and accumulation seasons, the SCFs even decrease with increases in slope.

### 4.3 Curvature

Figure 8 shows the mean snow cover fraction according to the different curvatures and aspects. As seen from the figure, the SCF in the concave or convex region (|curvature| >0.01) is larger than that in the flat region (|curvature| <0.01). From May to November, the SCF in the concave regions

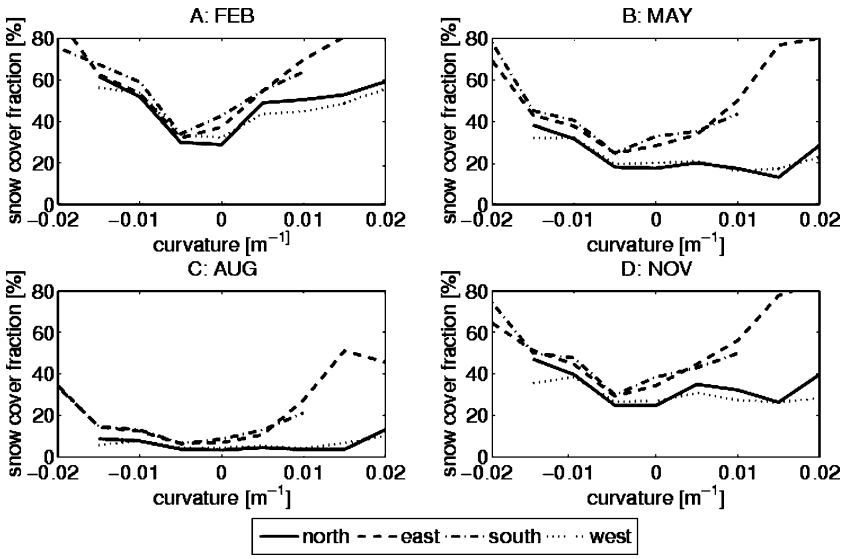


**Fig. 8** Mean SCF as a function of curvature in the different aspects during the snow maximum season (February), the ablation season (May), the minimum season (August) and the accumulation season (November). The *x*-axis is the curvature (units: $m^{-1}$) and the *y*-axis is the snow cover fraction (units: %)

(curvature >0) is larger than in the convex (curvature <0) regions, implying the snow cover is more likely to persist in the concave regions by shading solar radiation. In August, the majority of the snow cover in the southward and eastward slopes is maintained in the summits (convex regions) or valleys (concave regions).

### 4.4 Snowlines

Based on the high-resolution MODIS snow data, the evolution of snowlines over the TP can be explored for the first time. In this study, the snowline is defined as the elevation in which snow cover fraction is more than 50% (mostly snow covered). Figure 9 shows the mean elevation of snowlines in four different aspects.

In the winter, the snowline is lowest in northward slopes (roughly 2300 m) during January. Large snowline differences are shown for the four different directions. The snowline is roughly 3,000 m MSL minimum at southward slopes. It is consistent with the common concept that the snowline on the southward slopes is much higher than that on the northward slopes. In addition, the snowline on the windward slopes (westward slopes) is also lower than the snowline in the leeward slopes (east slopes). The range of variation of snowlines between different aspects is roughly 1,100 m.

From winter to summer, the snow cover melts and snowlines rise correspondingly. The snowline on northward slopes rises faster than in other directions and finally reaches 5,100 m. The snowline on the southward slopes, however, rises much slower and stops at 4,700 m MSL maximum. Consequently, the difference of snowlines in the four aspects reduces to 400 m. The annual variability of snowlines is largest in the northward slopes and smallest in the southward slopes.

Why is the snowline on the southward slopes lower than the northward slopes during the summer? It is speculated that this characteristic is possible as a result of special distribution of large mountains over the TP. The southward slopes are concentrated at the southern edge of the TP where sufficient air moisture and terrain lifting will produce deeper snow cover on the ground than in other regions. Although southward slopes receive more solar radiation during summer, the snow albedo effect could still cause a relatively lower snowline.

### 4.5 Snow ablation

Snow ablation is the main land-surface process during spring that influences the exchange of water and energy with the atmosphere. Figure 10 shows the day of onset of snow ablation averaged for different elevations and aspects. The onset date is defined as the Julian day on which the SCF is continuously decreasing for at least three 8-day periods after its peak in the winter.

At lower elevations, the snow ablation begins at the end of February. With increasing elevation, snow ablation is postponed accordingly in the middle of March at 3,000 m, April at 4,000 m and May above 5,000 m. At the same elevation, the snow melts later on the southward and eastward slopes due to deeper snow. Below 5,000 m, snow in the northward slopes melts roughly 10 days earlier, compared to the southward slope. The departure in the melting date between the different aspects disappears above 5,500 m.

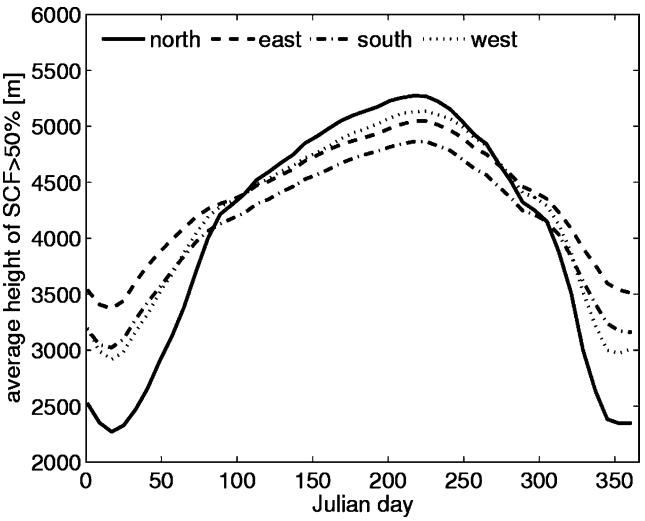


**Fig. 9** Annual evolution of snowlines in the four different aspects. The *x*-axis is Julian day and the *y*-axis is the elevation. The snowline is defined as the elevation in which the SCF is larger than 50%

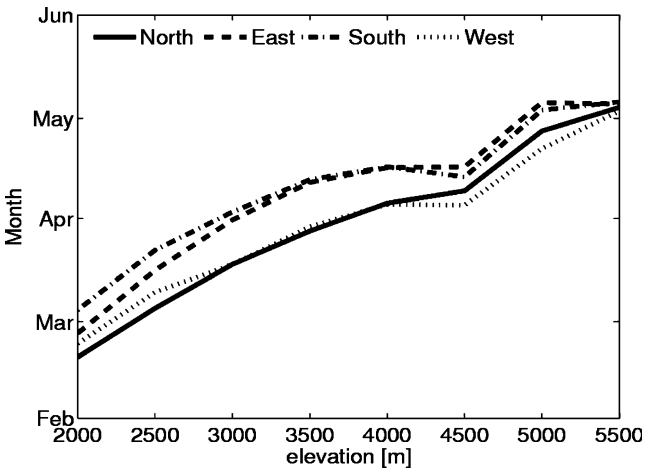


**Fig. 10** Snow-melting (ablation) date as a function of elevation in different aspects. The snow-melting date is defined as the Julian day on which the SCF begins continuous decreasing for at least three 8-day periods after its peak in the winter

## 5 Time trend, interannual variability, and snow-cover anomalies

### 5.1 Time trend

The reductions of snow cover and glacier due to global warming have been evidenced in the high mountains and the Polar region. Although short in length, the time series of the mean SCF over the whole TP from 2000–2006 was analyzed based on linear regression (Fig. 11). The linear trend in the mean SCF, for the whole period, is almost flat over the TP from 2000–2006, although a slight decreasing trend (about −0.34% per year) is found. The minimum SCF in each year also shows a negligible decreasing trend of −0.01% per year. The maximum of SCF, however, shows a notable decreasing trend of roughly −1.07% per year. From 2000 to 2006, the maximum of SCF is roughly reduced by 8%.

Although the minimum SCF over the whole TP does not show a clear decreasing trend, the snow-cover fraction above 5,000 m does show a notable decreasing trend in the snow minimum season (August) from 2000–2006 (figure not shown). The linear decreasing trend is relatively small in the area of 5,000–5,250 m (−0.26%/year), but increases with elevation. In the area of 5,750–6,000 m, the decreasing rate is largest (−0.58%/year). This decreasing trend is consistent with common speculation as to the response of snow cover to global warming over the TP.

With only 7 years of available MODIS data, however, it is hard to arrive at any definitive conclusion regarding the linear trend of the snow-cover fraction for this area. A longer time series of data is needed to attain more robust conclusions.

### 5.2 Inter-annual variability

In order to examine the interannual variability of the snow cover, Fig. 12 shows the variation of the mean SCF over the 7 years (2000–2006) with the elevation range in each month. In the snow maximum season (DJF), the SCF increases with elevation between 2,000–3,500 m, but shows a relatively lower value in the area between 4,000 and 5,000 m. Above 5,000 m, the SCF increases rapidly with elevation to the maximum (roughly 70%). The relatively lower value of SCF in the area of 4,000–5,000 m is due to the specific terrain features over the TP. The majority of area between 4,000 and 5,000 m is located in the interior of the TP, where available moisture is less, due to the topographic barrier effect of huge mountain ranges in the southern edge of the TP. The interannual variation of SCF is relatively large in the snow maximum season.

During the snow ablation season (MAM), SCF is significantly reduced in the lower elevation area (2,000–4,000 m) and has a relatively small interannual variability. In the area above 4,000 m, SCFs show a relatively large interannual variability, which is most evident in the area of 5,000–6,000 m. Above 6,000 m, the interannual variability is significantly reduced.

In the snow minimum season (JJA, especially the July and August), there is no significant snow cover in the area below 5,000 m. Most snow cover is located in the area above 5,000 m with small inter-annual variability. In the snow accumulation season (September and November), the SCFs are similar to the snow ablation season, increasing significantly in the area of 2,000–4,000 m with a relatively larger interannual variation.

### 5.3 Snow-cover anomalies

Snow-cover anomalies have been suggested as one of the slowly varying lower boundary forcings that cause climate fluctuation. The anomalous departure from the climatological mean would enhance or reduce snow albedo and hydrological effects that impact local or even remote climates. To quantify the snow-cover anomalies over the whole TP, a snow-cover anomaly index (SCAI) is defined as the *area average* of the anomalies of snow-

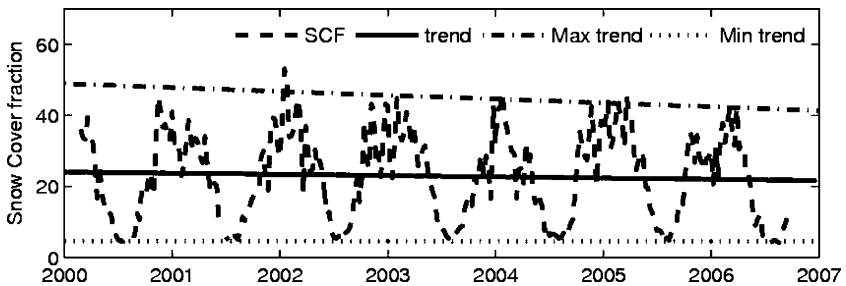


**Fig. 11** Time series of the average snow-cover fraction over the TP from the 2000 to 2006 (*blue dash*). The *blue line* shows the linear trend of the time series (−0.34%/year). The *green dash-dot line* shows the linear trend of the maximum SCF in the each snow year (−1.07% /year) and the *red dash line* shows the linear trend of the minimum SCF in each year (−0.01% /year)

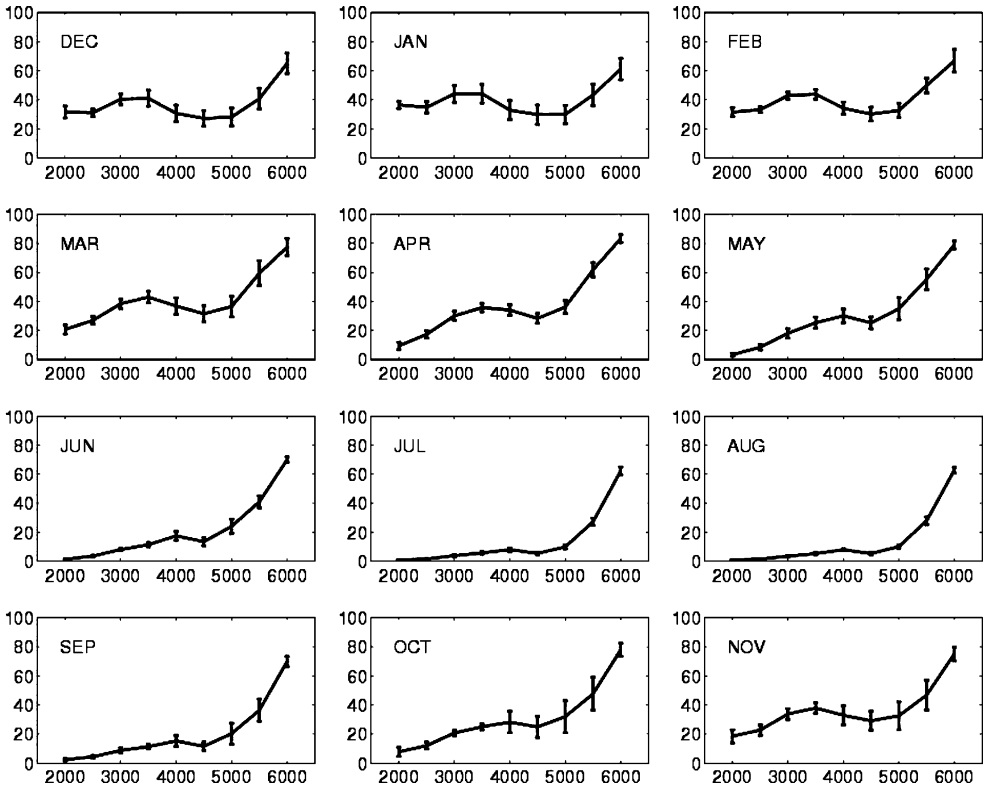


**Fig. 12** Mean SCF (*y*-axis) variation with different elevation height (*x*-axis) in each month. The *curve* on each panel shows the averaged SCF over the period of 2000–2006. The *error bars* show the standard deviation, indicating the variations of snow cover over the 2000–2006 period

cover fraction from seasonal climatological mean at each grid.

$$SCAI(t) = \frac{\int\int \left[ SCF(x,y,t) - \overline{SCF}\,(x,y,t_m) \right] dxdy}{\int\int dxdy} \qquad (3)$$

where SCF (x,y,t) represents the SCF at a certain grid and time and $\overline{SCF}(x,y,t_m)$ denotes the seasonal climatological mean of SCF at the same grid and based on averaged SFC for the period 2000–2006. The SCAI summarizes the anomalous extent of snow cover over a certain area in one index. SCAI also removes the seasonal cycle of snow cover so that it can be compared with the different seasons.

Figure 13 shows the longitudinal-time section of the SCAI along the main TP (30–40°N) from 2000–2006. In the spring of 2003 and 2005, the snow cover over the TP is more than normal (positive anomalies). In the same season of 2000 and 2004, the snow-covered area is obviously less than normal (negative anomalies). The large anomalies of snow cover concentrate in the winter and spring. In the summer, the anomalies are small and ignorable, usually less than 1%. The possible reason for the small anomalies is that snow melts rapidly after May.

The magnitude of interannual SCF anomalies in winter and spring are notable compared with the annual cycle. However, the large positive or negative anomalies do not generally persist for a period longer than 3 months.

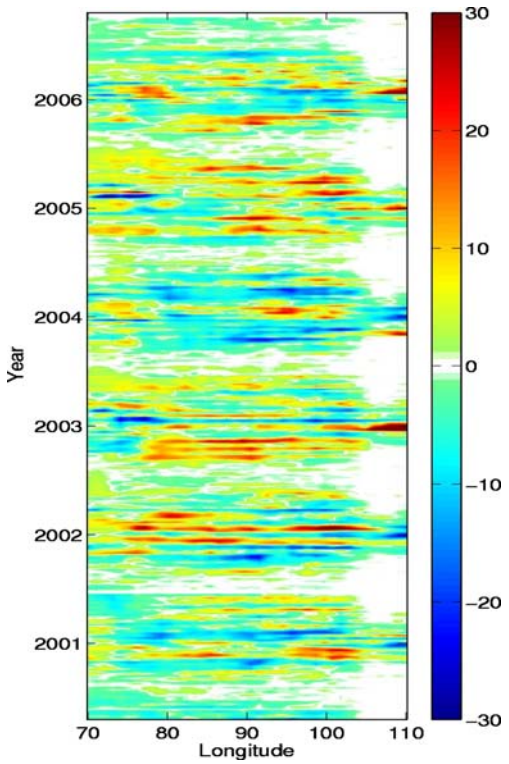


**Fig. 13** Longitude-time section of the SCAI along the main TP (30–40°N). The *x*-axis is longitude and the *y*-axis is time. The time resolution of snow-cover fraction is 8 days

The lack of persistence in snow-cover anomalies is also evidenced in the lag-correlation matrix of the mean snow-cover fractions during the 2000–2007 timeframe (table not shown). The autocorrelations of SCF are relatively larger (>0.50) only in the first or second lagged month. After 2 months, the lag-correlation becomes small or negative, implying that the snow-cover anomalies do not persist beyond this timeframe. The lag-correlations in June are almost negative with previous months, indicating the snow-cover anomalies do not persist to the summer.

## 6 Connection between snow-cover anomalies over the TP and the East Asian Summer Monsoon Onsets

As an ancient climatological concept, the monsoon is characterized by the seasonal reversal of prevailing surface winds, and alternation between a rainy summer and a dry winter (Ding 1993). The Asian summer monsoon defines essential features of the climate over Asia that have profound social and economic consequences. Studies on the annual cycle of the Asian summer monsoon, its onsets, as well as the variabilities of its intensity, have been an active research field (e.g., Wang 2006; Zhang and Li 2007; Li and Zhang 2008).

About 100 years ago, Blanford (1884) first speculated that the variability of continental snow cover might exert a thermal forcing on the land surface and consequently influence the Asian summer monsoon and its rainfall. Based on the Blanford's Hypothesis, Walker (1910) found a negative correlation between Himalayan snow depth at the end of May and the amount of summer rainfall over India between 1876 and 1908. In recent studies (Parthasarathy and Yang 1995; Yang 1996; Sankar-Rao et al. 1996; Bamzai and Shukla 1999; Kripalani and Kulkarni 1999), the snow-rainfall correlation is also significant.

Although there is no apparent relationship with the Indian monsoon, the snow cover over the TP is still believed to exert an influence on the summer rainfall over East Asia (EA). As EA is located in the downstream region of the TP, the snow-cover anomalies over the TP could exert a stronger thermal forcing on the East Asian Summer Monsoon (EASM). Accumulated evidence indicates that the relationship between snow cover and summer rainfall is rather complex. Although previous studies (e.g., Zhang and Tao 2001; Wu and Qian 2003) show a clear connection between winter snow cover over the TP and summer rainfall over EA, operational long-range forecasts made by the National Climate Center in China still fail to predict the summer rainfall over EA based on the snow depth observations in the winter.

With the large improvement in high-resolution MODIS snow mappings, specifically in the quantitative snow-cover fraction, the connection between snow cover over the TP with the EASM is reexamined. Although available MODIS snow data is short in length, its high accuracy and excellent consistency provide a more precise picture of snow-cover anomalies over the TP.

Based on the snow-cover anomaly index (SCAI) defined in the previous section, the spring snow cover over the TP is above normal in 2002, 2003, 2005, and 2006 (Table 1) but below normal in 2000, 2001, and 2004. The standard deviation of SCAI in spring is 2.74. If we classify the years with SCAI>±1.5 as the typically anomalous years, 2000 and 2004 are typically deficient snow-cover years (DS), while 2003 and 2005 are excessive snow-cover years (ES). In particular, 2004 displays significantly deficient snow cover in the spring, with the largest negative anomaly in March. In addition, 2005 shows significantly excessive snow cover in the spring, with three consecutive months in positive snow anomalies. In 2001, 2002, and 2006 the snow-cover anomalies are relatively small.

A dynamic monsoon index, also called western-north Pacific-East Asian monsoon index (EAMI), is selected to quantitatively describe the evolution of the East Asian summer monsoon. This monsoon index was originally defined by Wang and Fan (1999) as the difference of the 850-hPa mean westerly wind between a southern region (5–15°N, 100–130°E) and a northern region (20–30°N, 110–140°E) over the South China Sea. This dynamic

**Table 1** Snow-cover anomalies over the TP and EASM characteristics from 2000–2006

| | Snow-cover anomalous index (%) | | | | East Asian summer monsoon | | | |
|---|---|---|---|---|---|---|---|---|
| Year | Mar | Apr | May | MAM | Onset date (Julian day) | Withdrawal date (Julian day) | Spell (days) | EAMI (JJA) |
| 2000 | 1.49 | −3.37 | −3.59 | −1.82 | 126 | 313 | 187 | 4.08 |
| 2001 | −1.64 | 0.85 | −0.97 | −0.59 | 130 | 299 | 169 | 6.91 |
| 2002 | 0.11 | −0.8 | 3.61 | 0.97 | 144 | 290 | 146 | 5.68 |
| 2003 | 2.68 | 0.71 | 4.04 | 2.48 | 141 | 280 | 139 | 2.18 |
| 2004 | −9.33 | −3.45 | −2.82 | −5.2 | 137 | 299 | 162 | 6.98 |
| 2005 | 4.42 | 3.52 | 3.6 | 3.85 | 154 | 294 | 140 | 3.36 |
| 2006 | 2.28 | 2.54 | −3.86 | 0.32 | 133 | 307 | 174 | 4.72 |

monsoon index, based on a latitudinal differentiated westerly, reflects "not only the strength of the tropical westerlies but also the intensity of the low-level vorticity associated with Western Pacific subtropical high." (Wang et al. 2001).

Based on NCEP/DOE reanalysis II data, the onset and withdraw date of the EASM is defined by the Julian day, when the daily EAMI steadily (more than 5 days) becomes positive or negative. The monsoon spell is defined as the difference between the withdraw date and the onset date. From Table 1, the onset date of the EASM shows a good connection with snow-cover anomalies in spring over the TP. Of all the years considered in this study, the onset of EASM in the year 2000 is the earliest and the year 2005 is the latest. Compared with SCAI in spring (MAM), the positive snow anomaly years (2002, 2003, 2005, and 2006) correspond with the later onset of EASM, with the exception of 2006. The years with negative snow-cover anomalies (2000, 2001, and 2004) correspond to the earlier onset of EASM. In addition, although the SCAI is positive in spring 2006, it changes to negative in May 2006. If we made a conclusion based on the SCAI in May, the snow-cover anomalies would show a fairly good reversal association with the onset of EASM.

To further confirm the connection of snow-cover anomalies with the onset of the summer monsoon, the onset dates according to the different criteria (in addition to EAMI) are analyzed in the typically anomalous snow years. Based on the onset criteria: (1) mean 850 hPa U wind over the Bay of Bengal (BOB, 80–100°E, 5–15°N) steadily shift to the westerly wind (more than 5 days); (2) mean 850 hPa U wind over the southern region of the South China Sea (SCS, 110–120°E, 5–15°N); and (3) intensive rainfall onset over the SCS [mean daily rainfall >5 mm/day based on the TRMM 3B42 dataset (Huffman 2007)]. Figure 14 confirms that the onset of EASM is early in the deficient snow years and relative later in the excessive snow years.

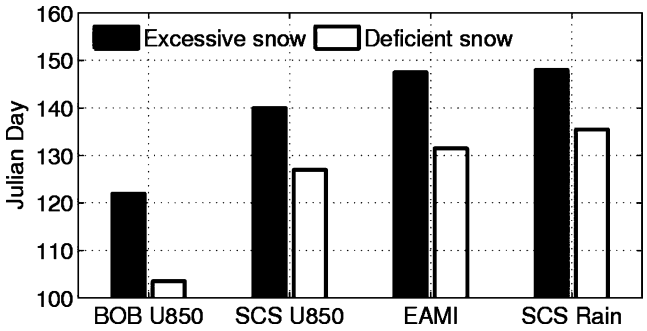


**Fig. 14** Mean onset date of EASM in the typical excessive snow (ES, positive anomaly) and deficient snow (DS, negative anomaly) years, based on the different criteria. *First and second column* are the onset date of westerly wind at 850 hPa in the Bay of Bengal (BOB) and the South China Sea (SCS). The *third column* is the onset date of EAMI and *fourth column* is the onset date of intense rainfall over SCS (mean daily rainfall >5 mm/day based on the TRMM 3B42 dataset)

## 7 Conclusions

Based on the MODIS quantitative satellite snow-cover fraction data products from 2000–2006, the snow-cover distributions, variations over the TP, and the connection between the snow-cover anomaly and EASM onset are analyzed in this study. The SCF is spatially quite inhomogeneous over the TP due to complex terrains. The most persistent snow cover occurs in the southern and western edges of the TP within large mountains and the west of Yarlung Zangbo Valley, where there is a strong link with the warm moist air that comes from southern Asia. In the interior of the TP, SCFs are relatively small and less persistent. The highest snow fractions, typically ranging from 49 to 76%, are mostly concentrated at elevations above 6,000 m. During the summer months (e.g., July and August), the TP retains approximately 5% snow cover made up of scattered patches of snow.

The spatial distribution of snow cover over the TP shows clear linkages with the terrain features. Generally speaking, SCFs increase with the elevation except in the interior of the TP. The SCFs in the southward and eastward slopes are commonly larger than those in the north- and west- facing slopes. The SCFs increase with the growth in steepness in the southward and eastward slopes, while they are not sensitive to incline in the northward and westward slopes. SCFs in the concave and convex regions are relatively larger than in the flat regions over the whole area. The annual evolution of snowlines shows distinguishing characteristics in the different aspects.

In addition, large interannual variabilities of snow cover occur in the late fall and winter months. Due to interannual variability, snow cover in each year shows large anomalies or deviations from the climatological mean. These anomalies, however, are limited in their duration, usually lasting less than 3 months. The anomalous snow cover in the winter does not persist to the summer season. There is an indication of slight decrease in the snow cover from 2000–2006. A longer time series of data, however, needs to be examined to reach a definitive conclusion about temporal trends.

The onset of the EASM is well associated with snow-cover anomalies in the spring and May. When there is excessive snow cover over the TP in May, the onset of EASM is later. In contrast, negative snow-cover anomalies are followed by an earlier onset of EASM.

The use of the multi-year MODIS snow-cover fraction data products eliminates the uncertainty due to inconsistencies in previous snow mappings. However, limited MODIS data in time length largely constrained the analysis in this study, especially in the time trend analysis and snow-monsoon relationship. More robust conclusions should be attained in the future when a longer time series of the data become available. Moreover, although the terrain feature-based

statistical distribution and variation of SCF in Sect. 4 could represent the SCF climate during the 7-year period, the subgrid (small) local slopes may be underestimated by the terrain features in this study due to the use of the CMG grid (roughly 5 km). Further detailed study will be made in the future.

**Acknowledgements** The authors are grateful to Dr. Jianping Li and two anonymous reviewers for their helpful comments and reviews. The authors also would like to thank Drs. Vincent Salomonson, James Steenburgh, and Jan Paegle for their valuable comments that greatly improved the first manuscript of this paper. The MODIS snow data used in this study are obtained from the National Snow and Ice Data Center (http://nsidc.org).

## References

Armstrong RL, Brodzik MJ (2001) Validation of passive microwave snow algorithms. Remote Sensing Hydrology (pp 87–93), [Proceeding of a symposium held at Santa Fe, New Mexico, USA, April 2000], IAHS Publ. no. 267

Bamzai AS, Shukla J (1999) Relation between Eurasian snow cover, snow depth, and the Indian summer monsoon: an observational study. J Climate 12:3117–3132

Blanford HF (1884) On the connection of the Himalayan snowfall with dry winds and seasons of drought in India. Proc R Soc Lond 37:3–22

Chang A, Foster JL, Hall DK (1987) Nimbus-7 SMMR-derived global snow cover parameters. Ann Glaciol 9:39–44

Chang A, Foster JL, Hall DK, Powell HW, Chien YL (1990) Nimbus-7 SMMR-derived global snow cover and snow depth data set. The Pilot Land Data System. NASA Goddard Space Flight Center, Greenbelt, MD, p 40

Che T, Li X, Gao F (2004) Estimation of snow water equivalent in the Tibetan Plateau using passive microwave remote sensing data (SSM/ I) (In Chinese). J Glaciol Geocryol 26:363–368

Cohen J, Rind D (1991) The effect of snow cover on the climate. J Climate 4:689–706

Dey B, Kathuria SN, Kumar OB (1985) Himalayan summer snow cover and withdrawal of the Indian summer monsoon. J Appl Meteor 24:865–868

Dickson RR (1984) Eurasian snow cover versus Indian monsoon rainfall—an extension of the Hahn–Shukla results. J Appl Meteor 23:171–173

Ding Y (1993) Monsoons over China. Kluwer Academic Publishers, p 432

Frei A, Robinson DA (1999) Northern hemisphere snow extent: regional variability 1972–1994. Inter J Climatol 19:1535–1560

Guo Y, Zhai P, Li W (2004) Snow cover in China, derived from NOAA Satellite Remote Sensing and Conventional Observation (In Chinese). J Glaciol Geocryol 26:755–760

Hahn DG, Shukla J (1976) An apparent relationship between Eurasian snow cover and Indian monsoon rainfall. J Atmos Sci 33:2461–2462

Hall DK et al (2001) Development of technique to assess snow cover mapping errors from space. IEEE Trans Geosci Remote Sens 39:432–438

Hall DK et al (2002a) MODIS snow cover products. Remote Sens Environ 83:181–194

Hall DK, Kelly REJ, Riggs GA, Chang ATC, Foster JL (2002b) Assessment of the relative accuracy of hemispheric-scale snow-cover maps. Ann Glaciol 34:24–30

Huffman GJ (2007) README for accessing experimental real-time TRMM multi-satellite precipitation analysis (TMPA-RT) data set. [Available online at ftp://trmmopen.gsfc.nasa.gov/pub/merged/3B4XRT_README.]

Jin M (2006) MODIS observed seasonal and interannual variations of atmospheric conditions associated with hydrological cycle over Tibetan Plateau. Geophys Res Lett 33:L19707. doi:10.1029/2006GL026713

Kanamitsu M, Ebisuzaki W, Woollen J, Yang S, Hnilo JJ, Fiorino M, Potter GL (2002) NCEP–DOE AMIP-II Reanalysis (R-2). Bull Am Meteorol 83:1631–1643

Kripalani RH, Kulkarni A (1999) Climatology and variability of historical Soviet snow depth data: some new perspectives in snow—Indian monsoon teleconnections. Climate Dyn 15:475–489

Li P-J (1993) Characteristics of snow cover in western China (In Chinese). Acta Geograph Sin 48:505–514

Li J, Zhang L (2008) Wind onset and withdrawal of Asian summer monsoon and their simulated performance in AMIP models. Climate Dyn. doi:10.1007/s00382-008-0465-8

Moore GWK (2004) Mount Everest snow plume: a case study. Geophys Res Lett 31:L22102. doi:10.1029/2004GL021046

Parthasarathy B, Yang S (1995) Relationships between regional Indian summer monsoon rainfall and Eurasian snow cover. Adv Atmos Sci 12:143–150

Pu Z, Xu L, Salomonson V (2007) MODIS/Terra observed seasonal variations of snow cover over the Tibet Plateau. Geophys Res Lett 34:L06706. doi:10.1029/2007GL029262

Qin D, Liu S, Li P (2006) Snow cover distribution, variability and response to climate change in western china. J Climate 19:1820–1833

Qu J, Gao W, Kafatos M, Murphy R, Salomonson V (2006) Earth Science Satellite Remote Sensing: Vol. I: science and instruments. Tsinghua University Press and Springer, p 500

Riggs GA, Hall DK, Salomonson VV (2003) MODIS Snow Products User Guide. [Available online at http://www.modis-snow-ice.gsfc.nasa.gov]

Sankar-Rao M, Lau K-M, Yang S (1996) On the relationship between Eurasian snow cover and the Asian summer monsoon. Int J Climatol 16:605–616

Walker GT (1910) Correlation in seasonal variation of weather 11. Mem Ind Meteor Dept 21:22–45

Walland DJ, Simmonds I (1997) Modeled atmospheric response to changes in Northern hemisphere snow cover. Climate Dyn 13:25–34

Wang B (2006) The Asian monsoon. Springer, Berlin Heidelberg New York, pp 373–397

Wang B, Fan Z (1999) Choice of South Asian summer monsoon indices. Bull Am Meteorol Sci 80:629–638

Wang B, Wu R, Lau K-M (2001) Interannual variability of Asian summer monsoon: contrast between the Indian and western North Pacific-East Asian Monsoons. J Climate 14:4073–4090

Wu T-W, Qian Z (2003) The relationship between the Tibetan winter snow and the Asian summer monsoon and rainfall: an observational investigation. J Climate 16:2038–2051

Yanai M, Li C, Song Z (1992) Seasonal heating of the Tibetan Plateau and its effects on the evolution of the Asian summer monsoon. J Atmos Sci 57:2374–2396

Yang S (1996) ENSO-snow-monsoon associations and seasonal-interannual predictions. Int J Climatol 16:125–134

Yeh T-C, Gao YX, Tang MC, Luo SW, Shen CB, Gao DY, Song ZS, Qian YF, Yuan FM, Li GQ, Ding YH, Chen ZT, Zhou MY, Yang KJ, Wang QQ (1979) Meteorology of Qinhai- Xizhang (Tibetan) Plateau (in Chinese). Science Press, Beijing, p 300

Zhang L, Li J (2007) Seasonal rotation features of wind vectors and application to evaluate monsoon simulations in AMIP Models. Climate Dyn. doi:10.1007/s00382-007-0327-9

Zhang S, Tao S (2001) Influence of snow cover over the Tibetan Plateau on Asian summer monsoon (in Chinese). Chin J Atmos Sci 25:372–390